

DYNAMIC BUCKLING ANALYSIS OF THIN-SHELL COMPOSITE STRUCTURES BASED ON ISOGEOMETRIC ANALYSIS

Huihui Qiu¹, Yujie Guo^{1,2}, Zhenyu Guan¹, Haotian Zhu¹, Yukai Pan¹

¹College of Aerospace Engineering, Nanjing University of Aeronautics and Astronautics, Nanjing 210016, China ²State Key Laboratory of Mechanics and Control for Aerospace Structures, Nanjing University of Aeronautics and Astronautics, Nanjing 210016, China

Abstract

The load carrying capacity of thin-walled structures is known to be significantly influenced by stability aspects such as buckling. A reliable prediction of buckling phenomena requires a robust and accurate analysis tool and consideration of a number of inherent structural imperfections which often dominate the overall non-linear elastic response. In this contribution, we studied the dynamic buckling problems of composite shell structures in the framework of isogeometric analysis considering geometric imperfections. Our approach exploits the higher order approximation and continuity properties of NURBS modelled shell structures and considers geometry features such as cut-outs, common in industrial applications. We will present several classical shell buckling problems to reveal and assess the reliability and accuracy of the isogeometric analysis approach for geometric imperfect thin-walled composite structures. Besides, different loading cases and stacking sequences are evaluated and their influence on the dynamic buckling behaviors of the composite shell structures are studied in detail.

 $\textbf{Keywords:} \ \ \text{dynamic buckling, isogeometric Kirchhoff-Love shell, trimming, composite, Generalized-} \alpha \ \ \text{time integration}$

1. Introduction

Composite shell structures are widely used in various engineering disciplines, such as aerospace, automotive etc. The stability problems of such structures received considerable amount of attention in the past due to the large discrepancies and scatters of the buckling loads between experimental and theoretical predictions [1-3]. The main reason behind this problem is the combined effects of nonlinearity and randomness of all source of imperfections [4–5]. In the past, the investigations of the shell buckling problems are mainly focused on the static case, while the effect of dynamic loads on the stability problems of composite shell structures are not yet clearly defined, especially for the novel variable stiffness composite shell structures.

Traditional finite element method (FEM) uses linear facet elements to represent model geometries. This approximation introduces additional geometric errors which is rather crucial for the buckling analysis of shell structures. Isogeometric analysis (IGA) [6] adopts non-uniform rational B-spline (NURBS) functions for both the representation of the geometry model and the approximation of the physical field. The higher order approximation and higher order continuity properties of NURBS make IGA an excellent candidate for the analysis of thin-walled structures where curved geometries are captured exactly. Compared to traditional FEM, isogeometric analysis eliminates the geometric discretization error which may have a significant influence on the buckling of imperfection sensitive structures.

The superiority of IGA has been demonstrated successfully in the field of shell buckling [7–10], where research works can be classified into two categories: static buckling analysis and dynamic buckling analysis. Dynamic approaches such as explicit dynamics, dynamic relaxation as well as implicit dynamics are widely used to study the post-buckling behaviors of shell structures. Compared to explicit methods, implicit approach is more stable and allow larger time steps. For buckling simulations, it is sometimes desirable for implicit schemes to have high frequency dissipation, while

in the low-frequency range, the dissipation effect is minimized. Generalized- α methods (including its variants) evaluate inertial, external and internal forces as a linear combination of the quantities at the start and end of the time step, thus are second-order accurate and high-frequency dissipative. Other implicit schemes with controllable numerical dissipation include: Generalized energy-momentum method, energy-decaying scheme etc.

In this paper, we extend our previous work on the isogeometric dynamic buckling analysis of isotropic shell structures to composite materials [11,12]. The higher order approximation and continuity properties of NURBS will be exploited, and geometric features such as cut-outs, common in industrial applications, will be included in the IGA framework. In addition, the influences of dynamic loading parameters and stacking sequences on the dynamic buckling behaviors of composite shells are investigated in detail.

The paper is organized as follows. The Kirchhoff-Love shell theory, governing equations, the isogeometric discretizations and trimmed element integrations are introduced in Section 2. Next, the Generalized- α time integration scheme and its linearizations are presented in Section 3. Several numerical results are presented in Section 4. Finally, we summarize the main findings and point out the future directions to complete the paper in Section 5.

2. Isogeometric Kirchhoff-Love Shell Element for trimmed geometries

2.1 Isogeometric Kirchhoff-Love Shell Element

In this section, the basic formulations governing the behavior of the Kirchhoff-Love shell element are presented. We note that, an upper case notation refers to the undeformed configuration, and a lower case notation refer to the deformed configuration. In addition, Greek indices take values 1, 2, Latin indices take values 1, 2, 3.

The governing equations of the geometrically nonlinear Kirchhoff-Love shell can be formulated as:

$$-\int_{A} (\mathbf{N} : \delta \boldsymbol{\varepsilon} + \mathbf{M} : \delta \boldsymbol{\kappa}) dA + \int_{A} P_{0} \cdot \delta \boldsymbol{u} dA + \int_{\Gamma} \boldsymbol{T}_{0} \cdot \delta \boldsymbol{u} d\Gamma = \int_{A} \rho h \ddot{\boldsymbol{u}} \cdot \delta \boldsymbol{u} dA$$
 (1)

where N is the membrane force, M is the bending moment, where $\delta \varepsilon$, $\delta \kappa$ and δu are the variation of the membrane strain, bending strain and displacement, respectively, where T_0 is the traction along the Neumann boundary Γ , P_0 is the surface load on the domain A, where ρ is the material density, h is the shell thickness, dA is the differential area in the reference configuration, where \ddot{u} is the acceleration of the shell.

The membrane strain tensor ε and bending strain tensor κ of Kirchhoff-Love shell are formulated, respectively, as:

$$\varepsilon = \varepsilon_{\alpha\beta} A^{\alpha} \otimes A^{\beta} \tag{2}$$

$$\kappa = \kappa_{\alpha\beta} A^{\alpha} \otimes A^{\beta} \tag{3}$$

where the components $\,arepsilon_{lphaeta}\,$ and $\,\kappa_{lphaeta}\,$ are written as

$$\varepsilon_{\alpha\beta} = \frac{1}{2}(a_{\alpha\beta} - A_{\alpha\beta}) \tag{4}$$

$$\kappa_{\alpha\beta} = B_{\alpha\beta} - b_{\alpha\beta} \tag{5}$$

where

$$a_{\alpha\beta} = \boldsymbol{a}_{\alpha} \cdot \boldsymbol{a}_{\beta}, \quad A_{\alpha\beta} = A_{\alpha} \cdot A_{\beta} \tag{6}$$

$$b_{\alpha\beta} = \mathbf{a}_{\alpha,\beta} \cdot \mathbf{a}_{\beta}, \quad B_{\alpha\beta} = A_{\alpha,\beta} \cdot A_{\beta} \tag{7}$$

where ${\it a}_{\alpha}$ and ${\it A}_{\alpha}$ represent the derivative of shell's mid-surface position vector $\overline{\it x}$ and $\overline{\it X}$ w.r.t. the parametric coordinate ξ_{α} , respectively, where ${\it a}_{\alpha,\beta}$ and ${\it A}_{\alpha,\beta}$ represent the derivative of ${\it a}_{\alpha}$ and ${\it A}_{\alpha}$ w.r.t. to the parametric coordinate ξ_{β} , respectively, and where ${\it a}_{3}$ and ${\it A}_{3}$ are the normal vector at shell's mid-surface.

Assume St. Venant-Kirchhoff constitutive model, the membrane force component $N_{\alpha\beta}$ and bending moment component $M_{\alpha\beta}$ can be written in Voigt notation as:

$$\begin{bmatrix} \overline{N}^{11} \\ \overline{N}^{22} \\ \overline{N}^{12} \end{bmatrix} = \overline{A} \begin{bmatrix} \overline{\varepsilon}_{11} \\ \overline{\varepsilon}_{22} \\ 2\overline{\varepsilon}_{12} \end{bmatrix} + \overline{B} \begin{bmatrix} \overline{\kappa}_{11} \\ \overline{\kappa}_{22} \\ 2\overline{\kappa}_{12} \end{bmatrix}$$
(8)

$$\begin{bmatrix}
\overline{M}^{11} \\
\overline{M}^{22} \\
\overline{M}^{12}
\end{bmatrix} = \overline{B} \begin{bmatrix} \overline{\varepsilon}_{11} \\
\overline{\varepsilon}_{22} \\
\overline{\varepsilon}_{12} \end{bmatrix} + \overline{D} \begin{bmatrix} \overline{\kappa}_{11} \\
\overline{\kappa}_{22} \\
\overline{\kappa}_{12} \end{bmatrix}$$
(9)

where $\overline{A}, \overline{D}$ are the extensional and bending stiffness, respectively, where matrix \overline{B} accounts for the coupling of membrane and bending actions and vanishes for symmetric stacking sequences, and where $\bar{\mathbb{Q}}$ sdenotes the quantities represented in the local Cartesian coordinate system.

Following the concept of IGA, the displacement u and its variation δu are discretized with the same NURBS basis as the shell's mid-surface \overline{X} :

$$\overline{X} = \sum_{i=1}^{n} R_i \mathbf{P}_i = \mathbf{R}^T \mathbf{P}$$
 (10)

$$\boldsymbol{u} = \sum_{i=1}^{n} R_i \boldsymbol{U}_i = \boldsymbol{R}^T \boldsymbol{U}$$
 (11)

$$\delta \boldsymbol{u} = \sum_{i=1}^{n} R_{i} \delta \boldsymbol{U}_{i} = \boldsymbol{R}^{T} \delta \boldsymbol{U}$$
 (12)

where R_i is the *i*-th NURBS basis, where P_i , U_i and δU_i represent the *i*-th control point vector, displacement vector and its variation, respectively, where R, P, U and δU are the corresponding vectors collecting the corresponding quantities.

Substituting Eqs.(11), (12) into Eq. (1), and leveraging the arbitrary nature of δU_i results in the discretized equilibrium equation:

$$f - r = M_a \ddot{U} \tag{13}$$

where f, r and M_a are the external force vector, inner force vector and mass matrix, respectively, and can be represented as:

$$f = \int_{A} \mathbf{R}^{T} \cdot \mathbf{P}_{0} dA + \int_{\Gamma} \mathbf{R}^{T} \cdot \mathbf{T}_{0} d\Gamma$$
(14)

$$r = \int \left(N : \frac{\partial \varepsilon}{\partial U} + M : \frac{\partial \kappa}{\partial U} \right) dA$$
 (15)

$$\boldsymbol{M}_{a} = \int_{A} \rho h \boldsymbol{R}^{T} \boldsymbol{R} dA \tag{16}$$

2.2 Trimmed Element Integration

The NURBS geometries are subject to tensor product constraints which are difficult to represent complex shapes. Trimming employs Boolean operations between objects thus provides a simple mechanism for the representation of complex geometries in CAD systems. For NURBS surfaces, trimming introduces additional trimming curves which are independent of the underlying parametric representations of the surface. The loose connection between trimming curves and surface parametric space brings additional difficulties for isogeometric analysis and special treatments are indispensable for the direct analysis of trimmed geometries.

In this paper, we employ a geometrically exact blending function method combined with a standard Gaussian integration scheme to handle the arbitrary shapes of trimmed element, cf. Figure 1. In blending function method, the trimming curve segments belonging to each trimmed element have to be extracted from the global trimming curves. Then we can define a mapping from the integration space $\{\hat{\xi}_1,\hat{\xi}_2\}$ to the trimming element in the parametric space $\{\xi_1,\xi_2\}$. For quadrilateral and triangular trimmed elements, the mapping can be defined, respectively, as:

$$\begin{bmatrix} \xi_1 \\ \xi_2 \end{bmatrix} = \frac{1}{4} ((1 - \hat{\xi}_1)(1 - \hat{\xi}_2) \mathbf{S}_1 + (1 - \hat{\xi}_1)(1 + \hat{\xi}_2) \mathbf{S}_4) + \frac{1}{2} \mathbf{C}_2(\hat{\xi}_2)(1 - \hat{\xi}_1)$$
(17)

$$\begin{bmatrix} \xi_1 \\ \xi_2 \end{bmatrix} = \frac{1}{4} ((1 + \hat{\xi}_1)(1 + \hat{\xi}_2) \mathbf{S}_2 + (1 - \hat{\xi}_1)(1 + \hat{\xi}_2) \mathbf{S}_4) + \frac{1}{2} \mathbf{C}_1(\hat{\xi}_1)(1 - \hat{\xi}_2)$$
(18)

where S_i , (i=1,2,3,4) are the corner points of the trimmed element in the parametric space, and where C_1 , C_2 are the trimming curve segments. The Jacobian matrix of the mapping from the Gaussian integration space to the parametric space of the trimmed element can be defined as:

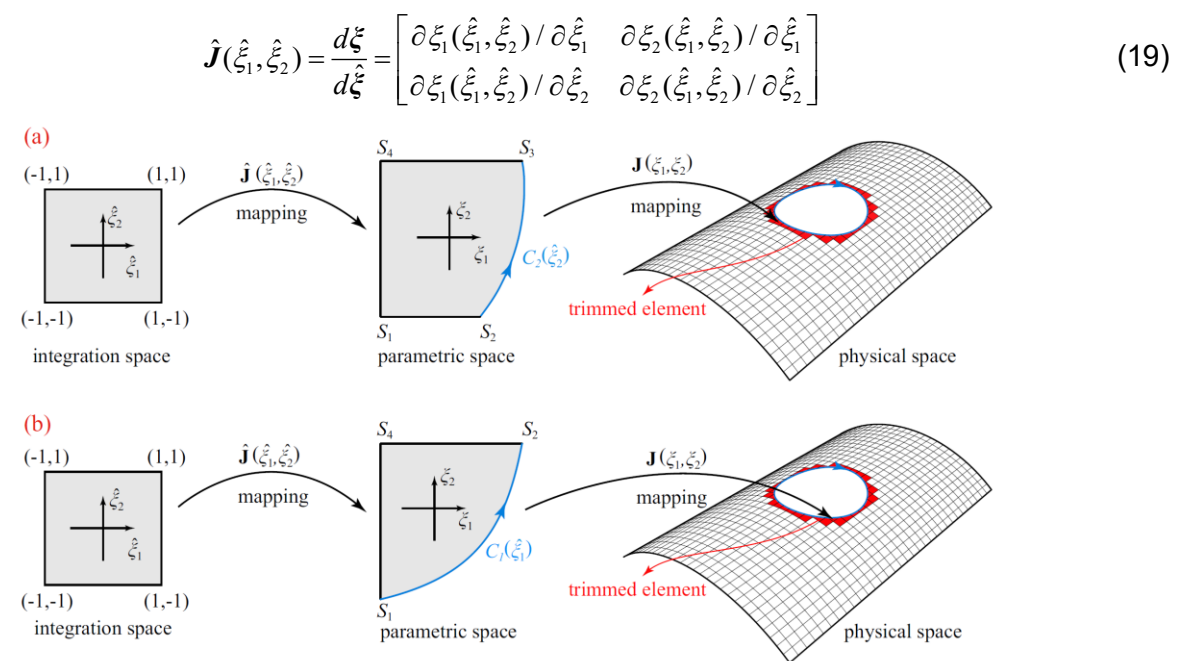


Figure 1 – The blending function method for trimmed elements: (a) quadrilateral trimmed element, (b) triangular trimmed element.

Based on the above mapping functions (17)-(18) and Jacobian matrix (19), the integration of trimmed element follows the standard way as the regular non-trimmed element. It is noted that, for trimmed elements with more complex shapes, we simply divide it into combinations of the quadrilaterals and triangles which are fall under the above strategy.

3. Generalized-α Time Integration Scheme

In this section, the Generalized- α time integration scheme used to discretize the time domain is introduced in Section 3.1. Then the linearization and iterative solution strategy of the governing equations is discussed in Section 3.2.

3.1 Generalized-α Time Integration Scheme

The Generalized- α time integration scheme evaluates the semi-discrete equilibrium equation Eq. (13) at general mid-points $t_{n+1-\alpha_{f}}$ and $t_{n+1-\alpha_{m}}$. The modified governing equations reads:

$$f_{n+1-\alpha_{c}} - r_{n+1-\alpha_{c}} = M_{a} \ddot{U}_{n+1-\alpha_{m}}$$

$$\tag{20}$$

where the subscripts in Eq. (20) represent the time discrete combinations of the corresponding quantities expressed as:

$$\ddot{U}_{n+1-\alpha} = (1 - \alpha_m) \ddot{U}_{n+1} + \alpha_m \ddot{U}_n \tag{21}$$

$$\mathbf{f}_{n+1-\alpha_f} = (1-\alpha_f)\mathbf{f}_{n+1} + \alpha_f \mathbf{f}_n \tag{22}$$

and where $r_{n+1-\alpha_s}$ is the algorithmic internal forces evaluated at the $U_{n+1-\alpha_s}$:

$$\mathbf{r}_{n+1-\alpha_f} = \mathbf{r}(\mathbf{U}_{n+1-\alpha_f}) \tag{23}$$

where

$$U_{n+1-\alpha_f} = (1 - \alpha_f)U_{n+1} + \alpha_f U_n$$
 (24)

Assuming Newmark's approximation, the accelerations and velocities at the end of the time step can be derived as:

$$\ddot{U}_{n+1} = \frac{1}{\beta \Delta t^2} (U_{n+1} - U_n) - \frac{1}{\beta \Delta t} \dot{U}_n - \frac{1 - 2\beta}{2\beta} \ddot{U}_n$$
 (25)

$$\dot{\boldsymbol{U}}_{n+1} = \frac{\gamma}{\beta \Delta t} (\boldsymbol{U}_{n+1} - \boldsymbol{U}_n) - \frac{\gamma - \beta}{\beta} \dot{\boldsymbol{U}}_n - \frac{\gamma - 2\beta}{2\beta} \Delta t \ddot{\boldsymbol{U}}_n$$
 (26)

The parameters α_f , α_m , β , γ are crucial for the stability and accuracy of the time integration scheme. They can be expressed as a function of the spectral radius at infinity $\rho_\infty \in [0,1]$, which controls the amount of numerical dissipation of the generalized- α time integration scheme. Their relationships are as following:

$$\alpha_f = \frac{\rho_{\infty}}{\rho_{\infty} + 1}, \quad \alpha_m = \frac{2\rho_{\infty} - 1}{\rho_{\infty} + 1}, \quad \beta = \frac{1}{(1 + \rho_{\infty})^2}, \quad \gamma = \frac{3 - \rho_{\infty}}{2(1 + \rho_{\infty})}$$
 (27)

Substituting Eqs. (25)-(27) into Eq. (20) results in the effective structural equation:

$$r(U_{n+1-\alpha_f}) + M_a \left(\frac{1-\alpha_m}{\beta \Delta t^2} (U_{n+1} - U_n) - \frac{1-\alpha_m}{\beta \Delta t} \dot{U}_n - \frac{1-\alpha_m - 2\beta}{2\beta} \ddot{U}_n \right) - f_{n+1-\alpha_f} = G(U_{n+1}) = 0$$
 (28)

3.2 Linearization and iterative solution procedure

The solution of the effective structural equation requires the linearization of Eq.(28) w.r.t. the displacement variables U_{n+1} which results in:

$$K_* \Delta U_{n+1}^{k+1} = -G(U_{n+1}^k)$$
(29)

where the superscripts k and k+1 represent iteration numbers in each time step, and where K_* is the effective stiffness matrix written as:

$$\boldsymbol{K}_* = (1 - \alpha_f) \boldsymbol{K}_T + \frac{1 - \alpha_m}{\beta \Delta t^2} \boldsymbol{M}_a$$
(30)

where $K_T = K_T(U_{n+1-\alpha_f}(U_{n+1}^k))$ is the deformation dependent algorithmic tangent stiffness matrix written as:

$$\mathbf{K}_{T} = \int_{A} \left(\frac{\partial \mathbf{N}}{\partial \mathbf{U}} : \frac{\partial \boldsymbol{\varepsilon}}{\partial \mathbf{U}} + \mathbf{N} : \frac{\partial^{2} \boldsymbol{\varepsilon}}{\partial \mathbf{U} \partial \mathbf{U}} + \frac{\partial \mathbf{M}}{\partial \mathbf{U}} : \frac{\partial \boldsymbol{\kappa}}{\partial \mathbf{U}} + \mathbf{M} : \frac{\partial^{2} \boldsymbol{\kappa}}{\partial \mathbf{U} \partial \mathbf{U}} \right) dA$$
(31)

Based on the above consistent linearization, Eq. (29) can be solved for each time step with Newton-Raphson iterations.

4. Numerical Examples

In this section, we test the accuracy and robustness of the proposed isogeometric dynamic buckling analysis framework with two preliminary numerical examples. The first example is the dynamic buckling of a cylinder with a cut-out, where the influence of cut-out on the dynamic stability properties is studied. The second example is the dynamic buckling of a composite cylinder under step pulse load, where influences of load amplitude and step size and stacking sequences on the dynamic buckling load of the cylinder are studied.

4.1 Dynamic Buckling of Cylinder with a Cut-out

In this example, the dynamic buckling of a cylindrical shell with a circular cut-out is studied. The geometric descriptions, material properties and loading histories are shown in Figure 2. The cylinder is subjected to an imposed z-direction displacement at the upper rim and fixed at the bottom rim. The cylinder consists of two patches with each patch being discretized with 64×40 cubic elements. The trimmed elements around the circular cut-out are integrated with blending function method which saves computational efforts compared to the fictitious domain based finite cell method. We set the spectral radius at infinity to be $\rho_{\infty}=0.6$, and use an adaptive time step size in the analysis which can be defined as:

$$\Delta t = (I_0 / I_n) \Delta t_p, \qquad I_n < I_{\text{max}}$$
(32)

where I_0 and I_{max} are the desired and maximum allowed number of iterations, respectively, Δt_p and I_n are the time step size and number of iterations of the last time step, respectively. It is noted that, in case $I_n \geq I_{\text{max}}$, the current time step size was re-computed with step size $\Delta t_p / 2$. For comparison, a reference solution was obtained from a 19418 S4R shell element discretization with ABAQUS [12].

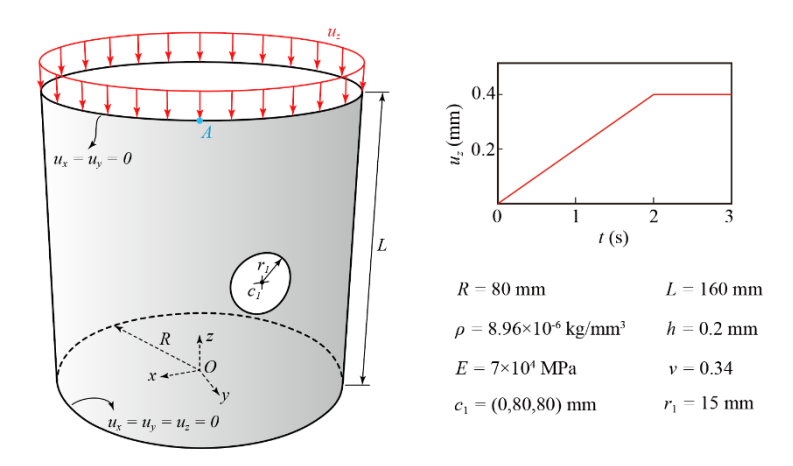


Figure 2 – Cylindrical shell with a cut-out: model descriptions, material properties and loading histories.

Figure 3 shows the load-displacement histories of the cylindrical shell for IGA and ABAQUS reference solutions, where good agreements can be observed. The buckling load obtained by IGA model is 5088.7 N, slightly lower than the ABAQUS model of 5171.7 N, which might due to the geometrically exact properties of the IGA model. In Fig. 4, displacement contour plots of the IGA solution at different post-buckling load stages are shown. It can be observed that, the buckling initiates around the circular cut-out with rapid change of local wrinkle patterns. After the initial buckling, two local dimples are generated which oscillates around the stable post-buckling state. This example demonstrates the flexibility and accuracy of the proposed isogeometric framework to deal with models with complex geometries and strong nonlinear responses.

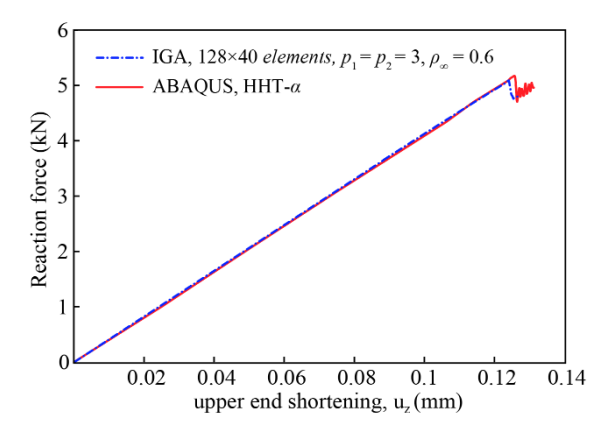


Figure 3 – Comparisons of load-displacement curve for the cylinder with cut-out.

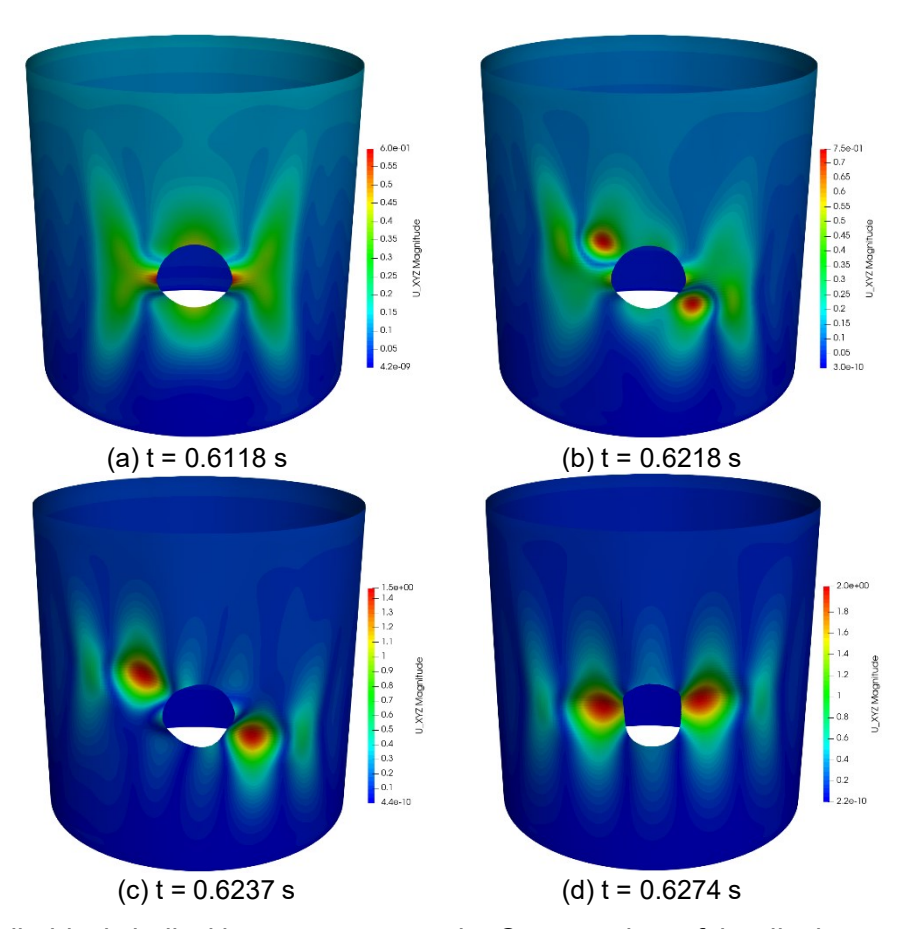


Figure 4 – Cylindrical shell with a cut-out example: Contour plots of the displacement at different time.

4.2 Dynamic Buckling of Composite Cylindrical Shell

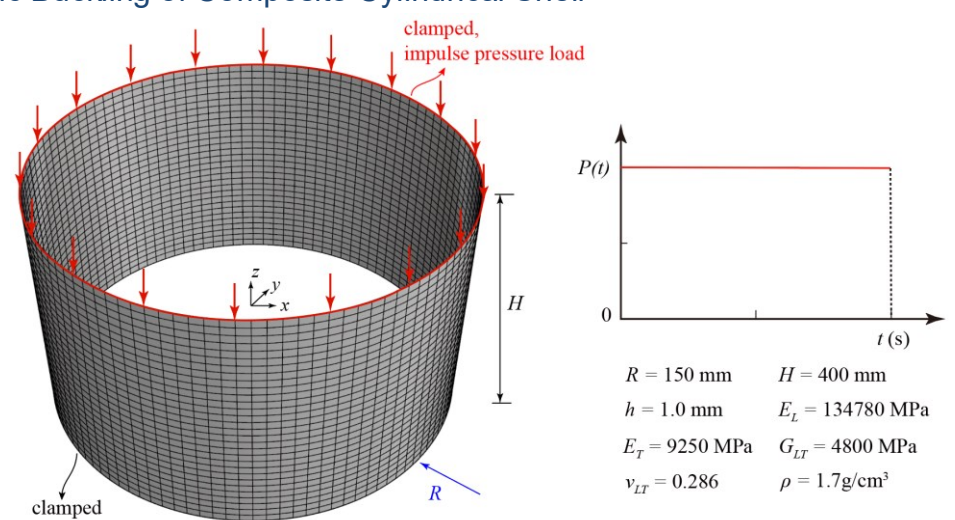


Figure 5 – Composite cylindrical shell: model descriptions, material properties, load and boundary conditions.

In this example, the dynamic buckling problem of a composite cylinder subject to a step pulse load is studied, cf. Figure 5. The bottom and top rims of the cylinder are fixed except for the axial degrees-of-freedom of the top rim. The composite cylinder has a length of 400mm, mean diameter of 300mm and a thickness of 1mm. Two types of stacking sequence are considered for the cylinder, which are [0/90/0/90/90/0] and [0/0/60/-60/-60/60/0/0]. The material properties of the carbon fiber reinforced composite are set to be $E_L = 134780$ MPa, $E_T = 9250$ MPa, $G_{LT} = 4800$ MPa, $V_{LT} = 0.286$, $\rho = 1.7$ g/cm³, t = 0.125 mm, where subscripts L and T represent fiber and its transverse directions, respectively, and where t is the thickness of each ply. The step pulse load is suddenly applied at the

top rim of the cylinder with a finite duration. The duration of the step pulse load are set to be 1ms, 2.5ms and 5ms. For each load time duration, we searching for the dynamic buckling load of the composite cylinder according to the Budiansky-Roth (B-R) criterion.

The cylinder consists of two patches with each patch being discretized with 56×42 cubic elements. We set the spectral radius at infinity to be $\rho_{\infty} = 0.6$, and use an adaptive time step size eq.(32) in the analysis. For comparison, a reference solution was obtained from a 15040 S4R shell element discretization with ABAQUS.

We first study the influence of load amplitude on the dynamic buckling behaviors of the composite cylinder. The load span is set to be 5ms, and both the stacking sequences are considered. The load displacement curves of the composite cylinder with two stacking sequences are plotted in Figure 6 and Figure 7, respectively. In Figure 6(a) and Figure 7(a), different load amplitudes are studied, which clearly shows the rapid change of displacement response with slight change of load amplitude. Based on the B-R criterion, the dynamic buckling load of the composite cylinder is 88KN and 113KN for stacking sequence of [0/90/0/90/90/90/0] and [0/0/60/-60/-60/60/0/0], respectively. Figure 6(b) and Figure 7(b) shows the comparison of the displacement responses between IGA and ABAQUS models. It can be observed that, IGA model predicts similar behavior compared to the ABAQUS model, except that, there is a slight phase difference between the two models, and the displacement predicted by IGA model is smaller than ABAQUS model. The above difference may due to the different time integration methods adopted in the two models. In ABAQUS model, HHT- α integration scheme is used, while in IGA model, generalized- α time integration method is used.

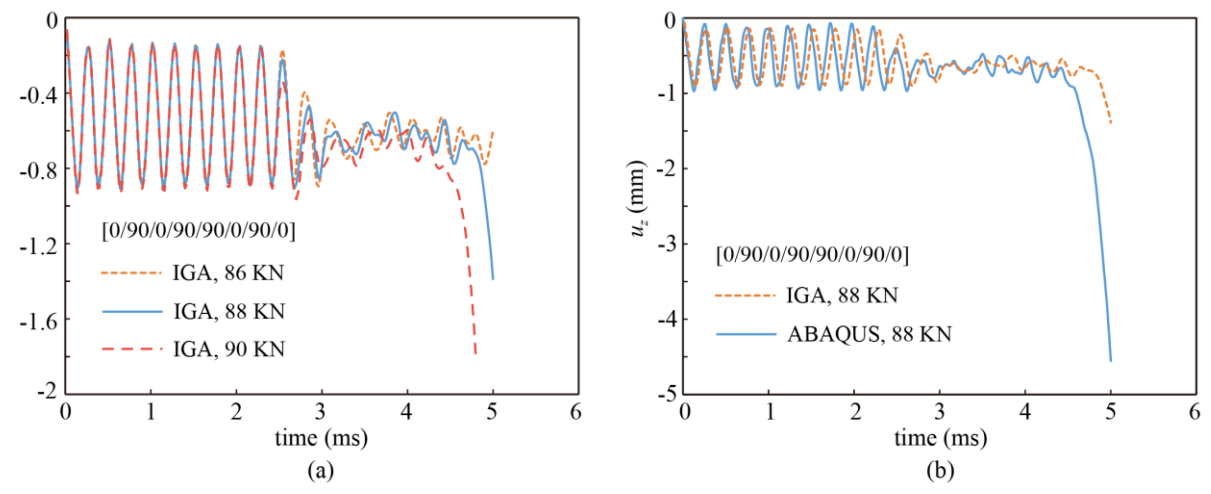


Figure 6 – Axial displacement histories of the [0/90/0/90/90/0] composite cylindrical shell under 5ms impulse step load: (a) influences of load amplitudes for IGA model (b) comparisons between IGA and ABAQUS model for load amplitude of 88KN.

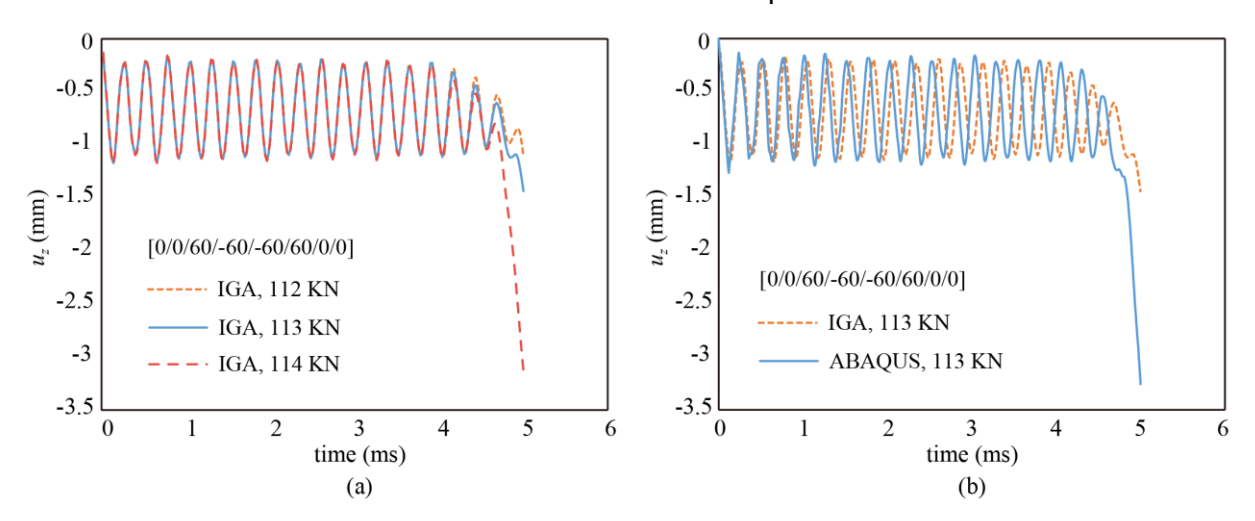


Figure 7 – Axial displacement histories of the [0/0/60/-60/-60/60/0/0] composite cylindrical shell under 5ms impulse step load: (a) influences of load amplitudes for IGA model (b) comparisons between IGA and ABAQUS model for load amplitude of 88KN.

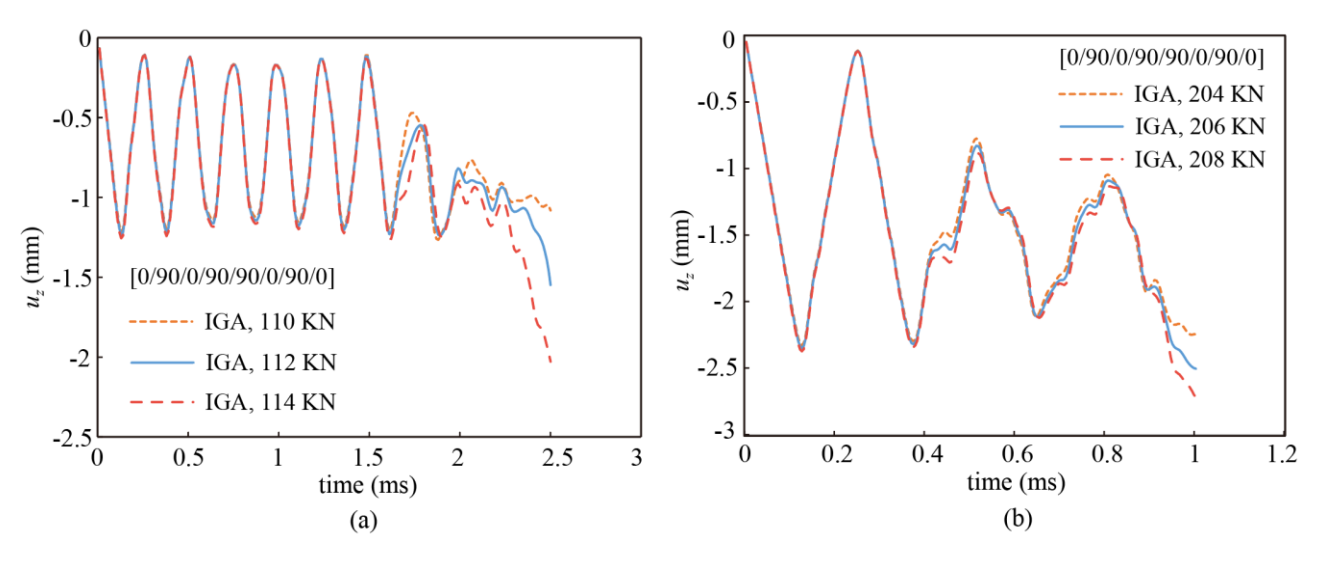


Figure 8 – Axial displacement histories of the [0/90/0/90/90/0] composite cylindrical shell under different load amplitudes: (a) load duration of 2.5ms (b) load duration of 1ms.

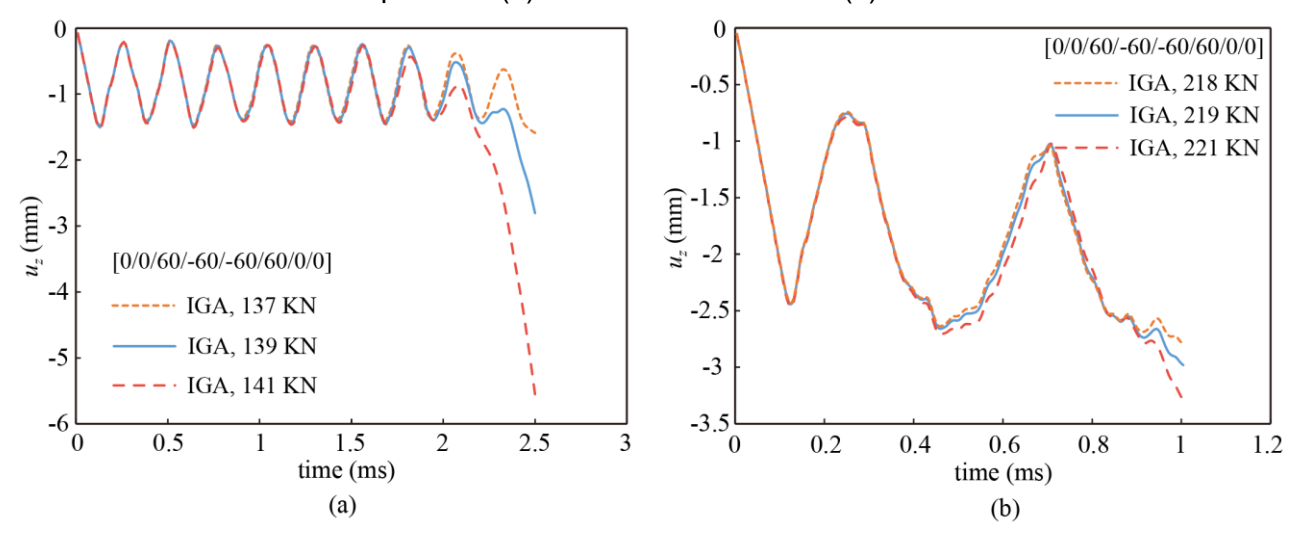


Figure 9 – Axial displacement histories of the [0/0/60/-60/-60/60/0/0] composite cylindrical shell under different load amplitudes: (a) load duration of 2.5ms (b) load duration of 1ms.

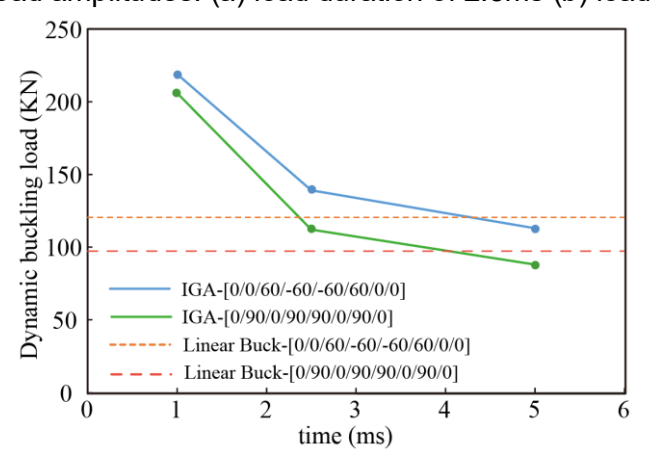


Figure 10 – Dynamic buckling loads for different time durations for cylindrical shells with stacking sequences of [0/90/0/90/90/0] and [0/0/60/-60/-60/60/0/0].

Figure 8 and Figure 9 show the axial displacement histories of the composite cylinder with different load amplitude and durations for the stacking sequence of [0/90/0/90/90/0/90/0] and [0/0/60/-60/-60/60/0/0], respectively. It can be observed that, the dynamic buckling loads of the composite cylindrical shell with [0/90/0/90/90/090/0] stacking sequence is 112KN for load duration of 2.5ms and 206KN for load duration of 1ms, respectively. In addition, the dynamic buckling loads for the stacking sequence of [0/0/60/-60/-60/60/0/0] is 139KN and 219KN for the load duration of 2.5ms and 1ms,

DYNAMIC BUCKLING COMPOSITE SHELL USING IGA

respectively. Besides, the comparisons of the buckling loads obtained with dynamic analysis and linear buckling analysis are shown in Figure 10. It can be observed that, for shorter load durations of 1ms and 2.5ms, the dynamic buckling loads are higher than the linear buckling loads. Especially for load duration of 1ms, the dynamic buckling loads are around 2 times higher than linear buckling loads. For longer load durations of 5ms, the dynamic buckling loads may be lower than the linear buckling loads, which indicates that, special attention should be paid on the dynamic stabilities of such shell structures at the design stage. In addition, the change of stacking sequences also has big influences on the dynamic buckling loads of the cylindrical shell, which indicates the potential of tailoring its dynamic behaviors with design optimization methods.

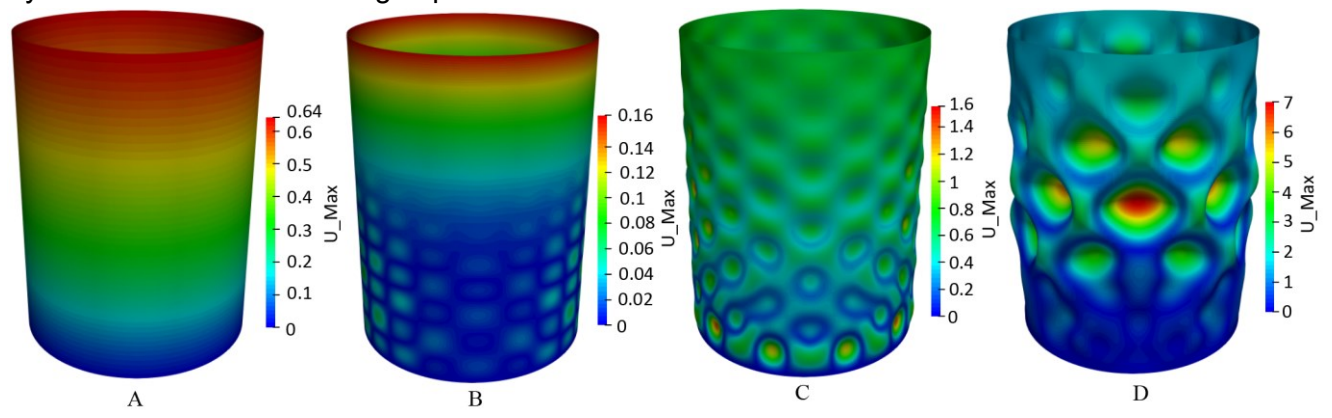


Figure 11 – Displacement contour plots for [0/90/0/90/90/0] composite cylindrical shells at different time steps, load duration is 5ms.

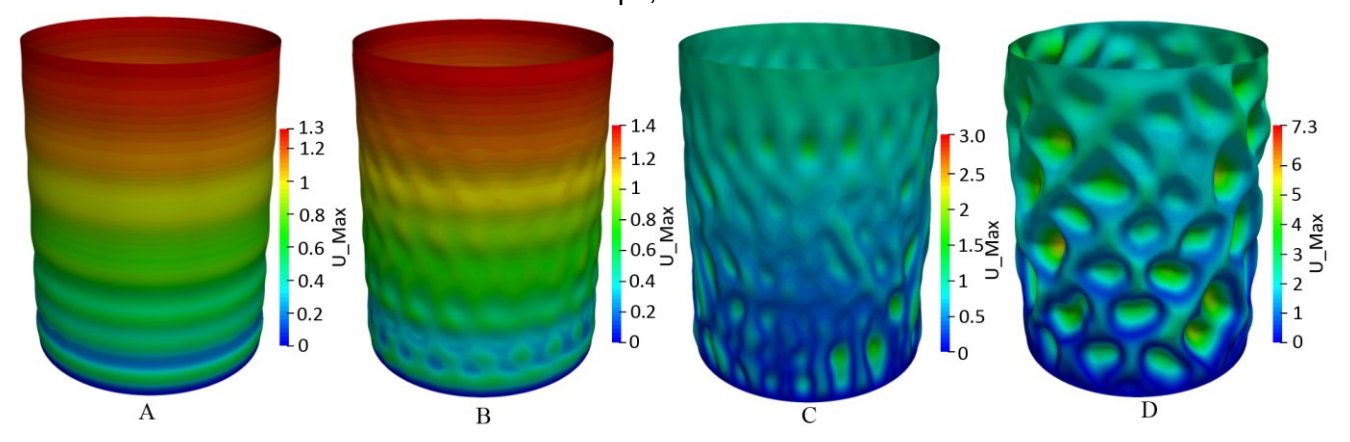


Figure 12 – Displacement contour plots for [0/0/60/-60/-60/60/0/0] composite cylindrical shells at different time steps, load duration is 2.5ms.

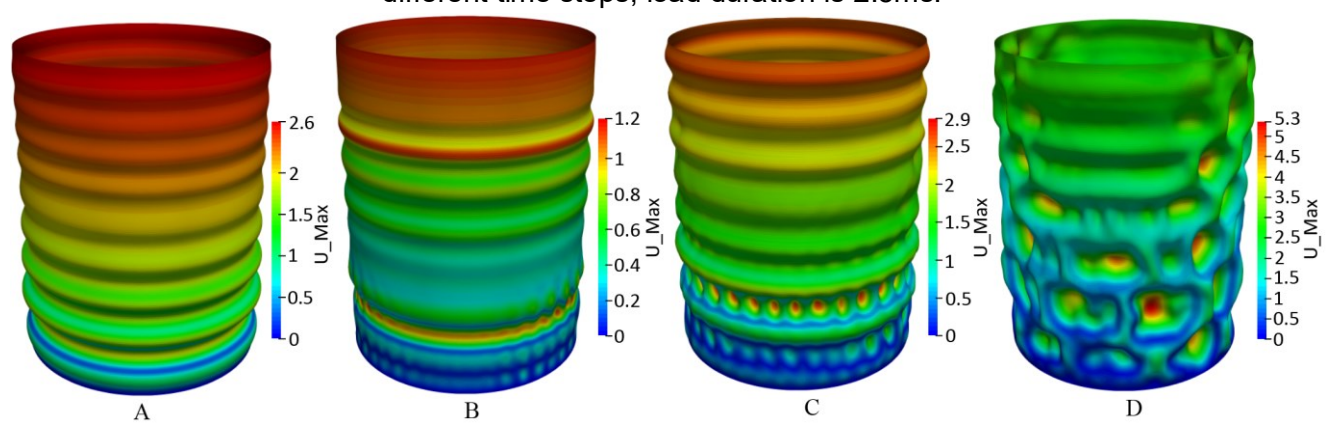


Figure 13 – Displacement contour plots for [0/0/60/-60/-60/60/0/0] composite cylindrical shells at different time steps, load duration is 1ms.

Figures 11~13 show the displacement contour plots of the cylindrical shell during dynamic buckling analysis. The load duration ranges from 5ms to 1ms, and different stacking sequences are also considered. It can be observed that, with the decrease of load duration, higher buckling modes may appear and dominates the dynamic buckling behaviors, which naturally leads to the higher buckling

loads.

5. Conclusion

In this paper, we propose a comprehensive framework for the dynamic buckling analysis of thin shell composite structures based on isogeometric analysis, where the influences of cut-outs, the amplitude and duration of step pulse load can be considered. We illustrated the performance of the proposed framework with two numerical examples including the buckling of a cylindrical shell with a cut-out and the dynamic buckling of a composite cylinder under step pulse load.

For the cylindrical shell with a cut-out example, we demonstrated that, cut-out features with arbitrary shapes can be naturally incorporated into the proposed framework, and strong nonlinear effects such as local wrinkles can be accurately captured.

For the composite cylindrical shell example, different load amplitudes, durations and stacking sequences are considered and their influences on the dynamic buckling behaviors of the cylindrical shell are studied. It is found that, the dynamic buckling load of the composite cylinder is much higher than its linear buckling loads for short load durations. Most importantly, the dynamic buckling loads can also be lower than its linear static buckling load, especially for longer load durations, which can be misleading when design such structures in dynamic situations. Besides, stacking sequences have a big influence on the dynamic buckling loads of the cylindrical shell, which indicates the potential of tailoring its dynamic behavior combined with design optimization methods.

Future work will be focused on the effects of different load types on the dynamic buckling behaviors of the cylindrical shell, and we will also study the design optimization problems of the cylindrical shell considering dynamic effects. Besides, the geometric imperfections can also be included in the analysis to fully explore the exact geometry description and higher order continuous properties of IGA.

6. Acknowledgement

The authors would like to thank the National Key R&D Program of China (Grant no. 2022YFB3302900) and National Natural Science Foundation of China (Grant no. 12472202) for their support.

7. Contact Author Email Address

mailto: yujiequo@nuaa.edu.cn

8. Copyright Statement

The authors confirm that they, and/or their company or organization, hold copyright on all of the original material included in this paper. The authors also confirm that they have obtained permission, from the copyright holder of any third party material included in this paper, to publish it as part of their paper. The authors confirm that they give permission, or have obtained permission from the copyright holder of this paper, for the publication and distribution of this paper as part of the ICAS proceedings or as individual off-prints from the proceedings.

References

- [1] Simitses G. Buckling and postbuckling of imperfect cylindrical shells: a review. *Applied Mechanics Reviews*, Vol. 39, No. 10, pp 1517–1524, 1986.
- [2] Arbocz J and Starnes Jr JH. Future directions and challenges in shell stability analysis. *Thin-Walled Structures*, Vol. 40, pp 729–754, 2002.
- [3] Elishakoff I. Uncertain buckling: its past, present and future. *International Journal of Solids and Structures*, Vol. 37, No. 46-47, pp 6869–6889, 2000.
- [4] Arbocz J and Babcock Jr CD. The effect of general imperfections on the buckling of cylindrical shells. *Journal of Applied Mechanics*, Vol. 36, No. 1, pp 28–38, 1969.
- [5] Papadopoulos V, Stefanou G and Papadrakakis M. Buckling analysis of imperfect shells with stochastic non-gaussian material and thickness properties. *International Journal of Solids and Structures*, Vol. 46, pp 2800–2808, 2009.
- [6] Hughes T, Cottrell J and Bazilevs Y. Isogeometric analysis: CAD, finite elements, NURBS, exact geometry and mesh refinement. *Computer Methods in Applied Mechanics and Engineering*, Vol. 194, pp 4135–4195, 2005.
- [7] Leonetti L, Magisano D, Liguori F and Garcea G. An isogeometric formulation of the koiter's theory for buckling

DYNAMIC BUCKLING COMPOSITE SHELL USING IGA

- and initial post-buckling analysis of composite shells. *Computer Methods in Applied Mechanics and Engineering*, Vol. 337, pp 387–410, 2018.
- [8] Guo Y, Do H and Ruess M. Isogeometric stability analysis of thin shells: from simple geometries to engineering models. *International Journal for Numerical Methods in Engineering*, Vol. 118, pp 433–458, 2019.
- [9] Hao P, Wang Y, Tang H, Feng S and Wang B. A NURBS-based degenerated stiffener element for isogeometric static and buckling analysis. *Computer Methods in Applied Mechanics and Engineering*, Vol. 398, pp 115 245, 2022.
- [10] Lavrenčič M and Brank B. Simulation of shell buckling by implicit dynamics and numerically dissipative schemes. *Thin-Walled Structures*, Vol. 132, pp 682–699, 2018.
- [11] Guo Y, Pan M, Wei X, Luo F, Sun F and Ruess M. Implicit dynamic buckling analysis of thin-shell isogeometric structures considering geometric imperfections. *International Journal for Numerical Methods in Engineering*, Vol. 124, pp 1055–1088, 2023.
- [12] Hibbit, Karlsson and Sorensen. *ABAQUS/Standard Analysis User's Manual*. Hibbit, Karlsson, Sorensen Inc., 2007.